SCALAR-FIELD PROBABILITY DENSITY FUNCTIONS AND CONDITIONAL EXPECTATIONS IN UNIFORMLY SHEARED TURBULENCE

Amir Behnamian
Department of Mechanical Engineering
University of Ottawa
Ottawa, Ontario, Canada
abehn103@uottawa.ca

Stavros Tavoularis
Department of Mechanical Engineering
University of Ottawa
Ottawa, Ontario, Canada
stavros.tavoularis@uottawa.ca

ABSTRACT

The statistical properties of the velocity and scalar fields, including all three scalar derivatives, were measured simultaneously in nearly-homogeneous, uniformly sheared turbulence with two passively superimposed, non-homogeneous, scalar fields, namely a thermal mixing layer and the plume of a heated line source. The scalar probability density functions were sub-Gaussian in both scalar fields and the velocity expectations conditioned on the scalar values were non-linear. The conditional scalar dissipation rate was strongly anisotropic and could not be surrogated by any of its three parts along the three axes.

INTRODUCTION

The formulation of statistical balance equations for the turbulent velocity and for transported scalars in terms of probability density functions (PDF) is an alternative to the more common approach, which is in terms of statistical moments. Although both approaches lead to open hierarchies of equations, the PDF approach has an advantage in reactive flows, because it can treat arbitrary chemical reactions exactly, whereas the moment approach requires the use of simplified models (Pope, 1985). Moreover, the scalar PDF equation does not require a closure model, other than models used for closing the velocity PDF equations. Nevertheless, the scalar PDF equations also contain terms that require modelling, in particular conditional expectations of the velocity fluctuations and the scalar dissipation rate (*i.e.*, the rate of destruction of scalar fluctuations) ε_θ, which are conditioned upon the value of the scalar fluctuation θ. The scalar PDF in turbulent flows and related issues have been the subject of much experimental and theoretical work, but several issues remain unresolved. In this article, we will address the following three important questions:

a) What is the shape of scalar PDF, particularly at large scalar fluctuations? is the scalar distribution Gaussian?

b) What are the shapes of the conditional expectations of the velocity components, conditioned upon the scalar value? are they linear?

c) What is the shape of the conditional expectation of the scalar dissipation rate, conditioned upon the scalar value? is the scalar field locally isotropic? if not, can ε_θ be represented by one of its three parts, particularly the streamwise one?

We have conducted an extensive experimental study to address these questions using new measurements obtained in specifically designed experimental setups with measurement methods that are capable of resolving accurately the fine structures of both the velocity and scalar fields. To avoid complications arising from turbulence inhomogeneity, the proximity of walls or external intermittency, we have considered scalar fields in nearly homogeneous, but strongly anisotropic, turbulence. In this article, we will discuss some representative results in two scalar fields, both of which are non-homogeneous: a thermal mixing layer (TML), in which the scalar fluctuations are fully mixed and depend on the local mean fields, and the plume of a line source (PLS), in which the scalar fluctuations maintain effects of the scalar injection process. These results fill a void existing in the literature and are expected to contribute to our understanding and modelling capability of passive scalar transport and mixing in turbulent shear flows.

LITERATURE REVIEW

Several experimental studies of passive scalar transport and mixing have been conducted in wind- and water tunnels, in statistically simple, approximately homogeneous turbulence, which includes grid turbulence (GT) and uniformly sheared flow (USF). In GT the turbulence is nearly isotropic and decays downstream, whereas in USF the turbulence is highly anisotropic and grows downstream. The simplest scalar field superimposed on the turbulence would also be an approximately homogeneous one, which can be
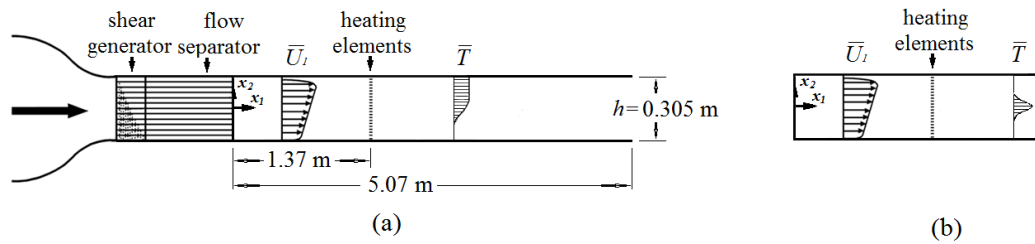
Figure 1: Schematic diagrams of the experimental facility showing the mean velocity and temperature profiles; (a) thermal mixing layer (TML); (b) plume of line source (PLS).

achieved by the injection of a scalar with either a uniform mean or a uniform transverse mean gradient. In the case with a uniform mean, there would be no production of scalar fluctuations and so any initial fluctuations would decay downstream. In contrast, the uniform scalar gradient would continuously produce scalar fluctuations.

Scalar PDF: The PDF of scalar fields with a uniform transverse mean gradient has been studied experimentally in both GT and USF. In GT produced by a conventional grid, it was found to have exponential tails (Jayesh & Warhaft, 1992; Gylfason & Warhaft, 2004), whereas, in GT produced by an active grid, it was sub-Gaussian (Mydlarski & Warhaft, 1998). In USF, the scalar PDF was found to be essentially Gaussian (Tavoularis & Corrsin, 1981a; Ferchichi & Tavoularis, 2002). The scalar PDF in non-homogeneous flows is known to exhibit complex behaviours. For example, in the centreline of the wake of a heated cylinder, the PDF in the far-field had an exponential tail towards the cold fluctuations and a Gaussian tail towards the hot fluctuations (Kailasnath et al., 1993).

Velocity conditional expectations: A common approach for modelling velocity conditional expectations is to assume that they depend linearly on the scalar value, which would be the case if the joint velocity-scalar distributions were jointly Gaussian (Pope, 1985). Tavoularis & Corrsin (1981a) showed that, for USF with a uniform mean temperature gradient, the joint PDF were Gaussian. The measured conditional expectations of the velocity in the same type of flow were generally consistent with the linear assumption (Ferchichi & Tavoularis, 2002). In GT with a constant mean temperature gradient, the velocity conditional expectations were found to be linear, despite the non-Gaussianity of the scalar PDF (Venkataramani & Chevray, 1978; Mydlarski, 2003). In GT with a scalar mixing layer (Li & Bilger, 1994), the conditional mean transverse velocity was approximately linear when the scalar was near the local mean-mixture fraction, but non-linear otherwise. Finally, in a confined wake flow (Feng et al., 2008), the conditional transverse velocity was approximately linear, but the conditional streamwise velocity was not.

Conditional expectation of the scalar dissipation rate: The scalar dissipation rate, defined as $\varepsilon_\theta = \varepsilon_{\theta 1} + \varepsilon_{\theta 2} + \varepsilon_{\theta 3}$, where $\varepsilon_{\theta i} = \gamma \overline{(\partial\theta/\partial x_i)(\partial\theta/\partial x_i)}$ (γ is the molecular or thermal diffusivity), has three components, which are equal to each other only in perfectly isotropic scalar fields, a condition that has never been met in practice. Among these three components, the streamwise one is the easiest one to measure (from time histories of the scalar and the use of Taylor's approximation). For this reason, in most

previous studies ε_θ has been approximated by $3\varepsilon_{\theta 1}$. The conditional expectation $\varepsilon_{\theta 1} | \theta$ in GT with a uniform mean scalar gradient was found to be ∪-shape behind a conventional grid (Jayesh & Warhaft, 1992) but ∩-shape behind an active grid (Mydlarski, 2003). These two shapes have been associated with super- and sub-Gaussian scalar PDF (Jayesh & Warhaft, 1992; Ching, 1993; Mydlarski, 2003). In the wake of a heated cylinder (Kailasnath et al., 1993), $\varepsilon_{\theta 1} | \theta$ was ∪-shape and diminished at negative fluctuations, thus resulting in a lobe shape on the cold side. In a jet of a fluorescent dye mixture (Kailasnath et al., 1993), the streamwise and transverse parts of the conditional dissipation rate had similar shapes and the authors argued that the shape of the total conditional expectation was the same as those of its parts. Mi et al. (1995) measured all three components of $\varepsilon_\theta | \theta$, but not simultaneously, in a slightly heated round jet; they found that local anisotropy was weaker near the jet axis and that all three parts of $\varepsilon_\theta | \theta$ were ∪-shape.

APPARATUS AND INSTRUMENTATION

All experiments were conducted in an open loop wind tunnel, having a test section that was 0.457 m wide, 0.305 m high, and 5.07 m long (see figure 1). Uniform mean shear was generated by an array of 12 parallel channels containing screens of varying solidity (shear generator) followed by a flow separator, which straightened the stream and ensured uniformity of the initial length scales; the spacing of these parallel channels was $M = 25.4$ mm. Passive heating of the flow was provided by a screen consisting of 49 ribbons (0.1×0.8 mm) of Nichrome alloy spaced by 6.1 mm in the transverse direction and inserted in the wind tunnel at 1.37 m downstream of the flow separator where the turbulence structure was fully developed. The TML was generated by heating electrically the upper half of the screen, whereas the PLS was generated by heating a single ribbon that was located near the wind tunnel centreline.

A three-wire probe consisting of a cross-wire and a cold-wire was used for simultaneous velocity and temperature measurements. The separations between neighbouring sensor planes were 0.5 mm. Tungsten wires with a diameter of 2.5 μm and a length to diameter ratio of 340 were spot welded to the cross-wire prongs and operated at a constant overheat ratio of 1.5. The cold-wire sensor was made of 90%Pt-10%Rh and had a diameter of 0.63 μm and a length to diameter ratio of about 950. A second probe, consisting of two orthogonal pairs of parallel cold-wires, was used to measure simultaneously the three temperature derivatives. The sensors in these probe had a diameter of 0.63 μm and length to diameter ratios of either 635 (those used for measuring the spanwise derivative) or 730 (those used for measuring the transverse derivative); the corresponding sensor
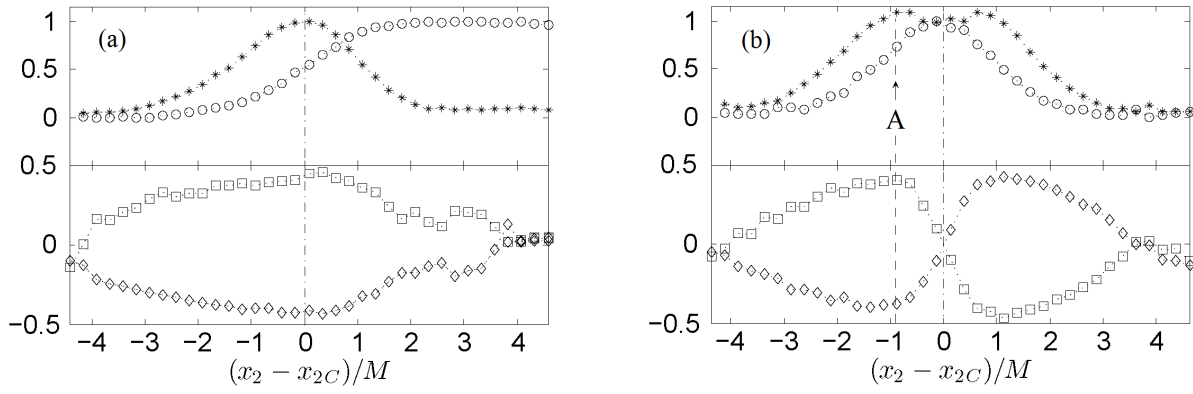
Figure 2: Time-averaged transverse profiles at $x_1/h = 10$ for (a) the TML and (b) the PLS; $\circ$: $\Delta\overline{T}/\Delta\overline{T}_m$; $*$: $\theta'/\theta'_{c\theta}$; $\square$: $\overline{u_1\theta}/(u'_1\theta')$ and $\diamond$: $\overline{u_2\theta}/(u'_2\theta')$; dash-dot lines represent the centres of the scalar fields; dashed line shows the location of measurements (point A) in the PLS; $\Delta\overline{T}_m = \overline{T}_m - \overline{T}_a$, where $\overline{T}_m$ is the maximum mean temperature and $\overline{T}_a$ is the mean temperature upstream of the heater; in the TML: $x_{2C}/M = 0.92$; in the PLS: $x_{2C}/M = 0.87$.

separation distances were 0.66 and 0.60 mm, respectively. Streamwise scalar derivatives were calculated using Taylor's approximation. The cold-wire sensors were operated at a current of 0.15 mA, which was sufficiently low for the velocity contamination of the cold-wire signals to be negligible. The -20 dB frequency cut-off for new cold-wires was estimated to be about 6 kHz. The hot- and cold-wire signals were low pass filtered at 10.4 and 8 kHz, respectively, and sampled simultaneously at a rate of 22 kHz. 1.1×10^8 samples were recorded at each measuring location, divided into 5000 blocks each of which was more than 200 velocity integral time scales long. Additionally, the cold-wire signals were filtered digitally using a double-pass, seventh-order, Butterworth, low-pass filter, with a cutoff adjusted at each location to the local Kolmogorov frequency.

RESULTS AND DISCUSSION

The turbulence: Time-averaged properties of the flow near the centres of the two scalar fields and far downstream of the heating screen ($x_1/h = 10$) are listed in the following table, in which L is the streamwise integral length scale, λ is the Taylor microscale and η is the Kolmogorov microscale.

$\overline{U}_{1c} = 7.48$ ms^{-1},	$\frac{d\overline{U}_1}{dx_2} = 31.2$ s^{-1},	$u'_1/\overline{U}_{1c} = 0.059$,
$\frac{\overline{u_1 u_2}}{u'_1 u'_2} = -0.46$,	$\overline{u_2^2}/\overline{u_1^2} = 0.43$,	$\overline{u_3^2}/\overline{u_1^2} = 0.65$,
$L = 41$ mm,	$\lambda = 6.8$ mm,	$\eta = 0.25$ mm,
$\varepsilon = 0.93$ m^{2}s^{-3},	Re$_\lambda = 194$,	
TML, centre:	$\Delta\overline{T}_m = 2.00$ K,	$\theta'/\Delta\overline{T}_m = 0.17$,
$\frac{\overline{u_1\theta}}{u'_1\theta'} = 0.45$,	$\frac{\overline{u_2\theta}}{u'_2\theta'} = -0.42$,	
$L_\theta/L = 0.55$,	$\lambda_\theta/\lambda = 0.60$,	
$\eta_\theta = 0.33$ mm,	$\varepsilon_\theta = 0.91$ K^{2}s^{-1},	
$\varepsilon_{\theta1}/\varepsilon_\theta = 0.22$,	$\varepsilon_{\theta2}/\varepsilon_\theta = 0.48$,	$\varepsilon_{\theta3}/\varepsilon_\theta = 0.30$,
PLS, point A:	$\Delta\overline{T}_m = 0.6$ K,	$\theta'/\Delta\overline{T}_m = 0.14$,
$\frac{\overline{u_1\theta}}{u'_1\theta'} = 0.41$,	$\frac{\overline{u_2\theta}}{u'_2\theta'} = -0.38$,	
$L_\theta/L = 0.51$,	$\lambda_\theta/\lambda = 0.60$,	
$\eta_\theta = 0.33$ mm,	$\varepsilon_\theta = 0.052$ K^{2}s^{-1},	
$\varepsilon_{\theta1}/\varepsilon_\theta = 0.20$,	$\varepsilon_{\theta2}/\varepsilon_\theta = 0.56$,	$\varepsilon_{\theta3}/\varepsilon_\theta = 0.24$.

The scalar fields: Figure 2 shows representative transverse profiles of the mean temperature rise $\Delta\overline{T}$ (normalized by the corresponding maximum $\Delta\overline{T}_m$), the temperature standard deviation θ' (normalized by the corresponding value $\theta'_{c\theta}$ in the "centre" of the scalar field) and the turbulent heat flux correlation coefficients for the two scalar fields. There is an apparent similarity of the two fields in one respect: the variations of these properties across the TML resemble those across either of the halves of the PLS, if symmetry is taken into consideration. The peaks in θ' in both cases occurred near an inflection point of the mean temperature profile, where also the turbulent heat fluxes acquired maximal magnitudes. Nevertheless, there is also an important difference between the two scalar fluctuation fields: in the TML, the temperature fluctuations in the cold and warm streams were very small and essentially negligible compared to $\theta'_{c\theta}$; in contrast, the temperature fluctuations in the PLS centre were significant and only slightly lower than $\theta'_{c\theta}$. This means that fluid that was heated by the ribbon persisted only partially mixed at the measurement location. Because of this difference, a comparison between the structures of the two scalar fields is expected to shed some light into the effect of initial condition. Such a comparison will be made in the following between the scalar properties at approximately the inflection points of the two mean fields, namely the centre of the TML and point A for the PLS (figure 2). The time-averaged properties of the temperature fields at these two locations have been included in the previous table. To explain the results that will be presented in the following sections, we need to know the extent of turbulent mixing across each scalar field. Turbulent transport mixes fluid with different temperatures over transverse distances that are at least equal to twice the transverse integral length scale of the transverse velocity fluctuation. The latter scale has been measured to be about $0.6L$ in USF (Vanderwel & Tavoularis, 2013), which is approximately equal to M for the present results. Consequently, one may infer that fluid can be transported to the centre of the TML from anywhere within the TML, including its edges with
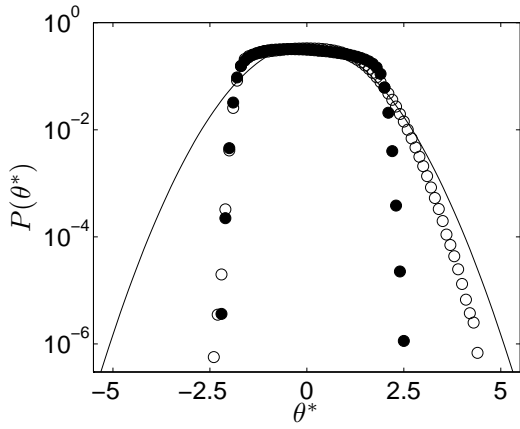
3

Figure 3: PDF of scalar fluctuations at the TML centre (●) and point A of the PLS (○); solid line represents a normal distribution; $\theta^* = \theta/\theta'$.

Figure 5: PDF of $\chi_\theta = (\phi - \overline{\phi})/\sigma_\phi$, where $\phi = \log e$, and σ_ϕ is its standard deviation, e is the instantaneous scalar dissipation rate ; symbols as in figure 3; solid line represents a normal distribution.

the cold and warm streams. In the case of point A in the PLS, fluid may be transported from the same side up to, and possibly beyond the edge of the cold stream, as well as from a considerable stretch of the other side, and certainly from the peak mean temperature region.

The scalar PDF: Figure 3 shows that the PDF of the scalar fluctuations in both fields were sub-Gaussian. In the TML centre, the PDF extended strictly to about $\pm 2.5\theta'$, which corresponds to the lower and upper temperature bounds, namely the temperatures of the cold and warm streams. This PDF has a very small skewness (-0.09) and a distinctly non-Gaussian flatness of 2.01. At point A of the PLS, the scalar PDF is almost identical to that in the TML centre on the cold side, but tends towards the Gaussian on the warm side. Non-zero values of the PDF were measured for positive fluctuations exceeding $4\theta'$, which is significantly larger than the maximum mean temperature rise and clearly demonstrates the presence of warm fluid originating in the thermal field of the heated ribbon. This creates a positive skewness of 0.18 and increases the flatness to 2.51.

Velocity conditional expectations: As shown in figure 4, at the centre of the TML, the expectations of the
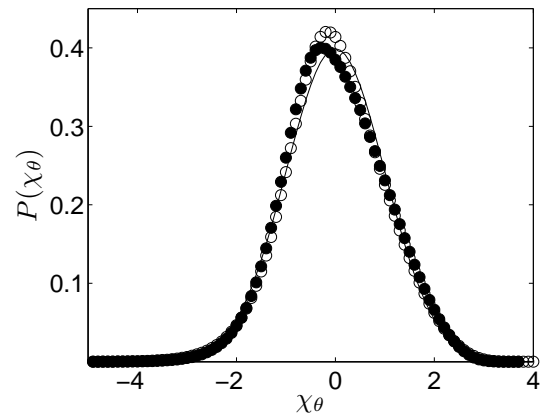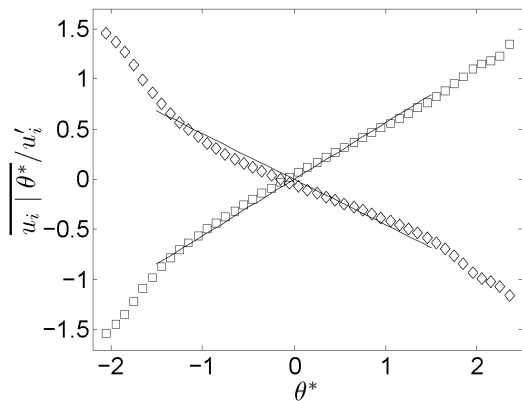
velocity components conditioned on the scalar fluctuations could be approximated by linear sections for $|\theta^*| \leq 1$ but deviated towards larger magnitudes for larger temperature fluctuations. This indicates that fluid particles that have very high or low temperatures are transported by particularly strong eddies, which are presumably capable of penetrating the local fluid that has average properties. At point A of the PLS, however, the velocity conditional expectations deviated measurably from linearity even in their central parts (figure 4) and had distinctly different appearances at their two ends. Towards the cold edge, large temperature fluctuations were transported by exceptionally strong eddies. In sharp contrast, towards the warm edge, large temperature fluctuations were transported by very weak eddies, in conformity with the previous observation that such fluctuations originated in the wake of the heated ribbon and therefore clustered near the PLS centre. These results show that initial conditions for the scalar field affect significantly the velocity conditional expectations.

PDF of the scalar dissipation rate and the scalar derivatives: The PDF of the standardized logarithm of the scalar dissipation rate for the two scalar fields are shown in figure 5. Except near the averages, both PDF collapsed
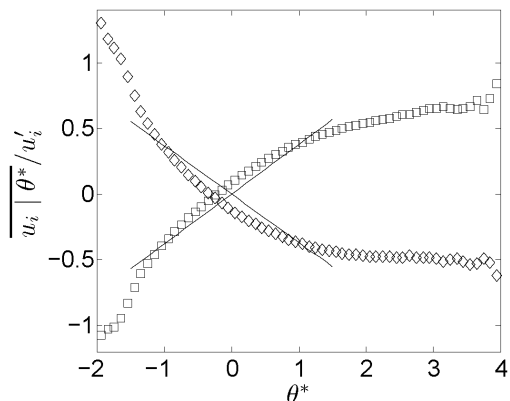

Figure 4: Conditional velocity expectations at the centre of the TML (left) and point A of the PLS (right) ; □: $i = 1$; ◇: $i = 2$; the slopes of the solid lines are equal to the corresponding turbulent heat flux correlation coefficients.
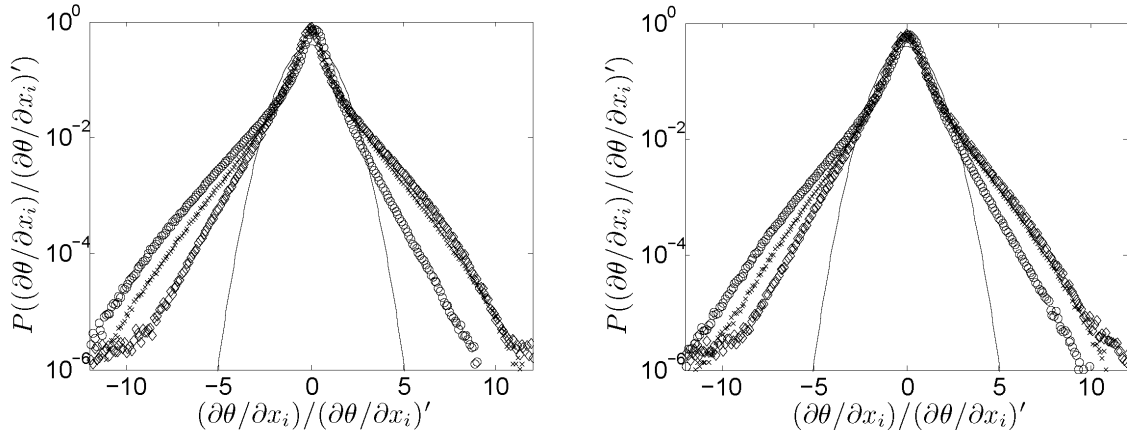
4

Figure 6: PDF of scalar derivatives at the centre of the TML (left) and point A of the PLS (right) at $x_1/h = 10$; ○: $i = 1$; ◇: $i = 2$; ×: $i = 3$; solid lines show a normal PDF.

on the Gaussian with the skewnesses and flatnesses being 0.03 and 3.2 in the TML and 0.04 and 3.1 in the PLS. This shows that the scalar dissipation rate was approximately log-normally distributed. The slight deviations from log-normality are consistent with previous observations (Eswaran & Pope, 1988; Jayesh & Warhaft, 1992). The PDF of the three scalar derivatives for the two scalar fields are presented in figure 6, with the corresponding skewness S and flatness F values listed in the following table. The streamwise derivative skewnesses were significant and negative, comparable with many results in the literature that indicate a cliff-ramp scalar structure. The transverse derivative skewnesses were positive, also compatible with the qualitative model of Tavoularis & Corrsin (1981b), by which both downward and upward eddies bring sudden rises of temperature in the positive x_2 direction. The spanwise derivative skewnesses were close to zero, as spanwise scalar ramps had no preferred orientation. All flatnesses were large, indicating that all scalar derivatives are highly intermittent.

	S_{TML}	S_{PLS}	F_{TML}	F_{PLS}
$\partial\theta/\partial x_1$	-0.94	-0.7	11.1	10.1
$\partial\theta/\partial x_2$	1.56	1.2	11.5	10.4
$\partial\theta/\partial x_3$	0.07	0.1	10.7	9.8

Conditional expectations of the scalar dissipation rate: The variations of the scalar dissipation rates and their three parts in the two scalar fields, conditioned on the scalar value, are shown in figure 7. In both fields, the scalar dissipation was strongly anisotropic, with the transverse part accounting for roughly half of the total and the spanwise part being somewhat larger than the streamwise one. These observations agree qualitatively with results in the literature (Gonzalez, 2000). The deviations of the conditional expectations from isotropy were lowest for near-average scalar values and generally increased with increasing fluctuation magnitude (figure 8). Focusing on the TML results first, one may observe that the conditional scalar dissipation and all its three parts had similar shapes: over a wide range around the average scalar value ($|\theta^*| \leq 2$),

they were ∩-shaped, but, for large scalar fluctuations, they turned locally ∪-shape. Nevertheless, the streamwise and transverse parts had very small values at large fluctuations, whereas the transverse part maintained strong magnitudes over the entire scalar value range. In summary, despite the qualitative similarities, the conditional scalar dissipation rate in the TML could not be approximated by a multiple of any of its parts. The differences between the behaviours of the conditional scalar dissipation parts were much stronger in the PLS, where they were not only quantitative, but also qualitative. In this case, the streamwise and spanwise parts were ∩-shape centrally and locally ∪-shape towards their two edges, like in the TML. On the contrary, the transverse part was very strongly ∪-shape in the entire scalar range. The total dissipation shape was affected visibly by the first two parts in the central range, but at large scalar fluctuations it was dominated by the transverse part. In summary, in the PLS the use of the streamwise part as a surrogate for the total scalar dissipation rate would be grossly inappropriate. Moreover, the shape of the conditional scalar dissipation rate cannot be consistently associated with sub- or super-Gaussianity of the scalar PDF.

CONCLUSIONS

Simultaneous hot-wire and cold-wire measurements have been made in two non-homogeneous scalar fields in uniformly sheared turbulence. These included a thermal mixing layer, in which scalar fluctuations were essentially the result of local conditions, and the plume of a line source, in which scalar fluctuations preserved initial condition effects. All results demonstrate that commonly employed simple models of various unknown terms in the scalar PDF equation would be inappropriate for non-homogeneous scalar fields, even in homogeneous turbulence. The scalar PDF were distinctly sub-Gaussian, more prominently so in the thermal mixing layer. The conditional velocity expectations were non-linear functions of the scalar fluctuations. The scalar dissipation rate was anisotropic, with the transverse part being much stronger than the streamwise and spanwise parts. The conditional transverse scalar dissipation part increased in importance for large scalar fluctuations. None of the three parts may act as a surrogate for the total conditional scalar dissipation rate.
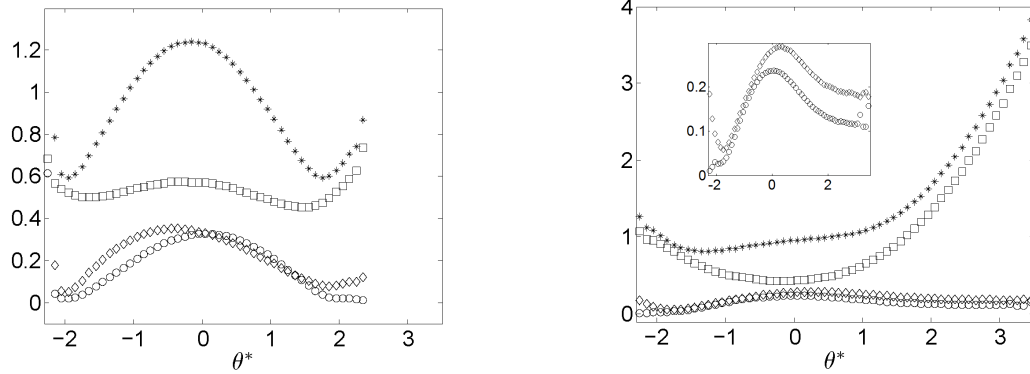
Figure 7: Conditional expectations of the scalar dissipation rate and its three parts at the centre of the TML (left) and at point A of the PSL (right); $*$: $(\varepsilon_\theta \mid \theta^*)/\varepsilon_\theta$; $\circ$: $(\varepsilon_{\theta 1} \mid \theta^*) / \varepsilon_\theta$; $\square$: $(\varepsilon_{\theta 2} \mid \theta^*) / \varepsilon_\theta$; $\diamond$: $(\varepsilon_{\theta 3} \mid \theta^*) / \varepsilon_\theta$; the inset shows details of the streamwise and spanwise parts.
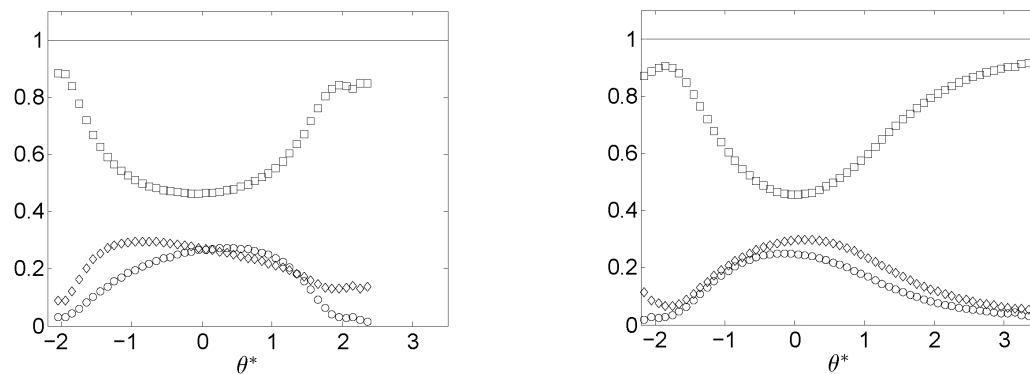

Figure 8: The ratios of conditional dissipation parts over the total at the centre of the TML (left) and at point A of the PSL (right); $\circ$: $(\varepsilon_{\theta 1} \mid \theta^*) / (\varepsilon_\theta \mid \theta^*)$; $\square$: $(\varepsilon_{\theta 2} \mid \theta^*) / (\varepsilon_\theta \mid \theta^*)$; $\diamond$: $(\varepsilon_{\theta 3} \mid \theta^*) / (\varepsilon_\theta \mid \theta^*)$.

REFERENCES

Ching, E. S. C. 1993 Probability densities of turbulent temperature fluctuations. *Phys. Rev. Lett.* **70**, 283286.

Eswaran, V. & Pope, S. B. 1988 Direct numerical simulations of the turbulent mixing of a passive scalar. *Phys. Fluids* **31**, 506.

Feng, H., Olsen, M. G., Fox, R. O. & Hill, J. C. 2008 Conditional statistics of passive-scalar mixing in a confined wake flow. *Phys. Fluids* **20**, 077105.

Ferchichi, M. & Tavoularis, S. 2002 Scalar probability density function and fine structure in uniformly sheared turbulence. *J. Fluid Mech.* **461**, 155–182.

Gonzalez, M. 2000 Study of the anisotropy of a passive scalar field at the level of dissipation. *Phys. Fluids* **12**, 2302.

Gylfason, A. & Warhaft, Z 2004 On higher order passive scalar structure functions in grid turbulence. *Phys. Fluids* **16**, 4012–4019.

Jayesh & Warhaft, Z. 1992 Probability distribution, conditional dissipation, and transport of passive temperature fluctuations in grid-generated turbulence. *Phys. Fluids* **4**, 2292–2307.

Kailasnath, P., Sreenivasan, K. R. & Saylor, J. R. 1993 Conditional scalar dissipation rates in turbulent wakes, jets, and boundary layers. *Phys. Fluids A* **5 (12)**, 3207.

Li, J. D. & Bilger, R. W. 1994 A simple theory of conditional mean velocity in turbulent scalar-mixing layer. *Phys. Fluids* **6(2)**, 605–610.

Mi, J., Antonia, R. A. & Anselmet, F. 1995 Joint statistics between temperature and its dissipation rate components in a round jet. *Phys. Fluids* **7**, 1665.

Mydlarski, L. 2003 Mixed velocity–passive scalar statistics in high-reynolds-number turbulence. *J. Fluid Mech.* **475**, 173–203.

Mydlarski, L. & Warhaft, Z. 1998 Passive scalar statistics in high-Péclet-number grid turbulence. *J. Fluid Mech.* **358**, 135–175.

Pope, S. 1985 Pdf methods for turbulent reactive flows. *Prog. Energy Combust. Sci* **11**, 119–192.

Tavoularis, S. & Corrsin, S. 1981*a* Experiments in nearly homogeneous turbulent shear flow with a uniform mean temperature gradient. Part 1. *J. Fluid Mech.* **104**, 311–347.

Tavoularis, S. & Corrsin, S. 1981*b* Experiments in nearly homogeneous turbulent shear flow with a uniform mean temperature gradient. Part 2. *J. Fluid Mech.* **104**, 349–367.

Vanderwel, C. & Tavoularis, S. 2013 Private communication.

Venkataramani, K. S. & Chevray, R. 1978 Statistical features of heat transfer in grid-generated turbulence: constant-gradient case. *J. Fluid Mech.* **86**, 513–543.